NUCLEAR SCIENCE AND TECHNIQUES **26**, 060201 (2015)

Simulation of high-intense beam transport in electrostatic accelerating column*

LU Xiao-Long (卢小龙),[1,2,†] YAO Ze-En (姚泽恩),[1,2] ZHNAG Yu (张宇),[1]
XU Da-Peng (徐大鹏),[1,2] CHEN Shang-Wen (陈尚文),[1,2] WANG Jun-Run (王俊润),[1]
HUANG Zhi-Wu (黄智武),[1] MA Zhan-Wen (马占文),[1] and WANG Wei (王伟)[1]

[1]*School of Nuclear Science and Technology, Lanzhou University, Lanzhou 730000, China*
[2]*Enginnering Research Center for Neutron Application, Ministry of Education, Lanzhou University, Lanzhou 730000, China*

(Received March 6, 2015; accepted in revised form June 9, 2015; published online December 20, 2015)

An electrostatic accelerating column was designed and fabricated by Lanzhou University for an intense D-T/D-D neutron generator. In order to achieve a neutron yield of 5.0×10^{12} n/s, a deuteron beam of 30 mA, accelerated to 400 kV, and transported in the electrostatic accelerating column smoothly are required. One particle-in-cell code BEAMPATH was used to simulate the beam transport, and the IONB1.0 code was used to simulate the intense beam envelopes. Emittance growths due to space charge effect and spherical aberration were analyzed. The simulation results show that the accelerating column can transport deuteron beam of 30 mA smoothly and the requirement for the neutron generator is satisfied.

Keywords: Electrostatic accelerating column, Intense beam, Simulation, Space charge

DOI: 10.13538/j.1001-8042/nst.26.060201

I. INTRODUCTION

In recent years, development of high-current ion accelerator have evoked considerable interest for various applications like accelerator-driven systems (ADS) [1], accelerator-based neutron sources [2], next-generation radioactive ion beam facilities [3], ion cancer therapy facilities [4, 5], etc. A D-T/D-D neutron generator which is a monoenergetic neutron source driven by an electrostatic accelerator is being developed by Lanzhou University. An electrostatic accelerating column for accelerating and transporting high-intense beam was designed and installed on the neutron generator. In order to achieve a neutron yield of 5.0×10^{12} n/s, a deuteron beam of 30 mA, accelerated to 400 kV and transported in the electrostatic accelerating column smoothly, is required [6, 7].

This paper aims to analyze and simulate the transport of high-intense deuteron beam in the electrostatic accelerating column for the D-T/D-D neutron generator. BEAMPATH [8], a well proven code using the PIC method, is used to carry out the beam transport simulations and investigate the emittance growth due to space charge effect [9] and spherical aberrations [10] in the electrostatic accelerating column, and a computer code named IONB1.0 for simulating intense beam envelopes which based on K-V equation has been developed and used.

II. ANALYSIS OF BEAM EMITTANCE GROWTH

A. The accelerating column

The accelerating column is 1370 mm in length (Fig. 1). It consists of the accelerating zones of A1 and A2, both being the size of Φ90 mm × 110 mm. They can be seen as two electrostatic lenses. Two electrodes biased negatively are installed on the accelerating column exit, for repelling secondary electrons back into the accelerating column and keeping them free from the ion source. Between the two electrodes is a permanent magnet lens at ground potential. The magnet lens and electrodes form a space charge lens [11], so as to prevent beam diverging excessively, and adjust the size of beam envelope at the accelerating column exit.

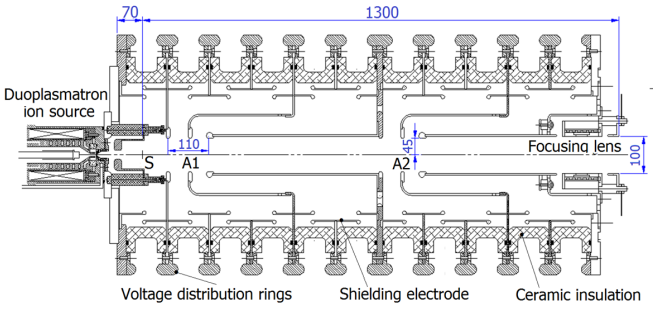

Fig. 1. (Color online) Schematic diagram of the accelerating column.

B. Effects of spherical aberrations

In general, transport of space charge dominated beam is analyzed in linear approximation method. In the presence of linear focusing field, the beam emittance remains constant.

* Supported by the National Nature Science Foundation of China (Nos. 11027508 and 21327801), Ministry of Sciences and Technology of China (No. 2013YQ040861) and Fundamental Research Funds for the Central Universities (No. lzujbky-2015-bt07)
† Corresponding author, luxl@lzu.edu.cn

Realistic focusing elements possess strong aberrations, resulting in distortion of phase space area occupied by the beam. Among others, the spherical aberration cannot be eliminated, hence the most significant effect on particle dynamics. The spherical aberration coefficient C_s is defined as [10, 12]

$$C_s = (f/r)^3 \Delta r, \tag{1}$$

where, f is the local length, r is the radial distance of an incident ray parallel to the axis, and Δr is the radial distance at the paraxial-image plane.

The change of slope of particle trajectory can be written via focal length f and aberration coefficient C_s [10, 12].

$$\Delta(\mathrm{d}x/\mathrm{d}y) = -(x/f)\left[1 + C_s(r/f)^2/f\right]. \tag{2}$$

Assume the initial beam distribution is described by the ellipse

$$\frac{x_0^2}{R^2}\varepsilon + \frac{x_0'^2}{\varepsilon}R^2 = \varepsilon, \tag{3}$$

where, R is the envelope size of beam, and ε is the beam emittance.

The transformation from initial particle variables before lens (x_0, x_0') to that after the lens (x, x') is given by

$$x = x_0, \tag{4}$$

$$x' = x_0' - \left(1 + \frac{C_s}{f}r_0^2\right)\frac{x_0}{f}. \tag{5}$$

Change variables (x, x') to action-angle variables (J,Ψ)

$$\frac{x}{R}\sqrt{\varepsilon} = \sqrt{2J}\cos\Psi, \tag{6}$$

$$\left(x' + \frac{x}{f}\right)\frac{R}{\sqrt{\varepsilon}} = \sqrt{2J}\sin\Psi. \tag{7}$$

Then beam ellipse distortion:

$$T + T^2 2\upsilon \sin\Psi\cos^3\Psi + T^3\upsilon^2\cos^6\Psi = 1, \tag{8}$$

where, $T = 2J/\varepsilon$ and $\upsilon = C_s R^4/(\varepsilon f^4)$. Without nonlinear perturbation, $\upsilon = 0$, the shape of beam emittance is round. While phase space areas occupied by beam before and after lens are the same, the effective area, occupied by the beam, is increased. The beam emittance can be estimated as a total area of elements $\mathrm{d}x\mathrm{d}x'$ occupied by the beam. Actual areas of the beam in both cases are the same, but the number of elements covered by the beam at phase pane is different. The increase of effective beam emittance as a square of product of minimum and maximum values of T:

$$\varepsilon_{\mathrm{eff}}/\varepsilon = (T_{\max}T_{\min})^{1/2}, \tag{9}$$

where $T_{\max}$ and $T_{\min}$ are determined numerically. Dependence of emittance growth versus parameter υ can be approximated by

$$\varepsilon_{\mathrm{eff}}/\varepsilon = \left(1 + K\upsilon^2\right)^{1/2}, \tag{10}$$

where $K \approx 0.4$. Finally, effective beam emittance growth due to spherical aberrations can be approximated by

$$\varepsilon_{\mathrm{eff}}/\varepsilon = \left[1 + K\left(C_s R^4/f^4\right)^2\right]^{1/2}. \tag{11}$$

C. Aberrations of space charge effect

Space charge density and space charge field of the beam of Gaussian distribution in free space are given by [13, 14]

$$\rho(r_0) = \frac{2I}{\pi R_0^2 \beta c}\exp\left(-2\frac{r_0^2}{R_0^2}\right), \tag{12}$$

$$E_b = \frac{I}{2\pi\varepsilon_0\beta c r_0}\frac{1}{r_0}\left[1 - \exp\left(-2\frac{r_0^2}{R_0^2}\right)\right], \tag{13}$$

where, ε_0 is permittivity of vacuum; I is the beam current; and $\beta = \upsilon/c$, υ is the particle velocity and c is the light speed in vacuum.

Nonlinear function in space charge field can be expanded as

$$f(r_0) = 1 - \exp\left(-2\frac{r_0^2}{R_0^2}\right) \approx 2\frac{r_0^2}{R_0^2} - 2\frac{r_0^4}{R_0^4} + \cdots. \tag{14}$$

At the initial stage of beam emittance growth we can assume, that particle radius does not change, while the slope of the trajectory changes. Then, we have the following nonlinear transformation:

$$r = r_0, \tag{15}$$

$$r' = r_0' + \frac{2zP^2}{R_0^2} - \frac{2zP^2}{R_0^4}r_0^3, \tag{16}$$

where, $P^2 = 2I/(I_c\beta^3\gamma^3)$ is the generalized perveance, γ is relativistic factor, and $I_c = 4\pi\varepsilon_0 mc^3/q$ is the characteristic beam current.

Use the same way as above, effect of spherical aberration on beam emittance can be determined as

$$\upsilon = \frac{4}{\beta^3\gamma^3}\frac{I}{I_c}\frac{z}{\varepsilon}. \tag{17}$$

Therefore, space charge induced beam emittance growth in free space is

$$\varepsilon_{\mathrm{eff}}/\varepsilon = \left[1 + \kappa\left[I/\left(I_c\beta^3\gamma^3\right)\right]^2(z/\varepsilon)^2\right]^{1/2}, \tag{18}$$

where, z is the drift length and $\kappa = 0.6$ is beam uniformity for Gaussian beam.

III. ENVELOP SIMULATION BASED ON K-V EQUATION

A. High-current ion beam envelope equation

For designing the intense neutron generator, a computer code of IONB1.0 was developed. Assuming a continuous, elliptically symmetric particle beam, its dynamics can be modeled by the $K-V$ (Kapchinsky–Vladimirsky) coupled-envelope equations [13, 15, 16]. Let the z coordinate represents the position along the design trajectory, and the x-y

plane is the transverse plane for the particle beam, we have the high-current beam envelope equation [17]:

$$\begin{cases} X'' + \dfrac{\varphi'}{2\varphi}X' + \dfrac{\varphi''}{4\varphi}X + K_x X - \dfrac{2\Pi}{X+Y} - \dfrac{\varepsilon_{x_0}^2\varphi_0}{X^3\varphi} = 0 \\ Y'' + \dfrac{\varphi'}{2\varphi}Y' + \dfrac{\varphi''}{4\varphi}Y + K_y Y - \dfrac{2\Pi}{X+Y} - \dfrac{\varepsilon_{y_0}^2\varphi_0}{Y^3\varphi} = 0 \end{cases}, \tag{19}$$

where, $X(z)$ and $Y(z)$ are dimension of the semi-axes of beam envelope in the x and y planes, respectively. The prime indicates differentiation with respect to z. φ, φ' and φ'' are the generalized potential, the electric field strength and the derivative of electric field strength at z axis (Beam axis), respectively. K_x and K_y refer to the focusing functions of transport elements in the x and y directions respectively. φ_0 is the normalized potential, ε_{x_0} and ε_{y_0} are the normalized emittances of beam on the (x, x') and (y, y') phase planes respectively. 2Π is the generalized perveance, it reflects space charge effect of the high-intense beam, and can be calculated by following formulas

$$2\Pi = \frac{I(1-F)}{2\pi\varepsilon_0}(2\eta)^{-\frac{1}{2}}\varphi^{-\frac{3}{2}}, \tag{20}$$

where, I is the beam current, F is the factor of space charge compensation, η is the charge-to-mass ratio of charged particle, and ε_0 is the permittivity of vacuum.

B. Numerical simulation method

For calculating X, the $K-V$ equation can be expressed as

$$X'' = -\frac{\varphi'}{2\varphi}X' - \frac{\varphi''}{4\varphi}X - K_x X + \frac{2\Pi}{X+Y} + \frac{\varepsilon_{x_0}^2\varepsilon_0}{X^3\varphi}. \tag{21}$$

As in Fig. 2, the z axis is divided into a series of micro-units, Δz. When Δz is tiny enough, we may approximately hold that X'' is a constant A in each micro-unit.

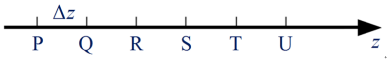

Fig. 2. Divided diagram for the beam axis.

After the beam passes through a Δz, its envelope and divergence may be approximately calculated by Eq. (22)

$$\begin{cases} X' = A\Delta Z + B \\ X = \dfrac{1}{2}A\Delta Z^2 + B\Delta Z + C \end{cases}, \tag{22}$$

where, A, B and C can be fixed by the initial conditions of beam envelope. As in Fig. 2, if the initial conditions at point P are (X_P, X'_P), in that case, $B = X'_P$ and $C = X_P$. A can be calculated by Eq. (21). The beam parameters at next interval point $Q(X_Q, X'_Q)$ are determined by Eq. (22). Then, Q is regarded as the start point, we can calculate the beam parameters at next point $R(X_R, X'_R)$. So long as Δz is tiny enough, the better consults of beam parameters can be got at each interval point. The same method is used to calculate the Y.

IV. BEAM SIMULATION

A. Optimization accelerating column fields

The distribution of electric fields is not only to meet the requirements of increasing beam energy and inhibiting beam divergence excessively, but also to make 400 kV voltage have a reasonable allocation to avoid local field strength be too large to produce discharge. Using the POISSION/SUPERFISH code [18, 19], the distribution of equipotential surface was simulated as shown in Fig. 3, the electric field strengths in all regions are less than half of its maximum value of the breakdown electric field strengths, the electric field directions are marked by the arrows. Figure 4 shows the map of radial fields $E_r(z, r)$ and $E_z(z, r)$ at 0–4 cm radii.

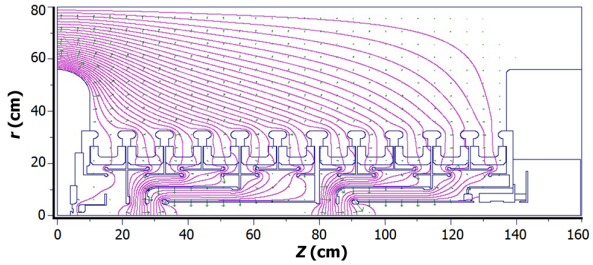

Fig. 3. (Color online) Equipotential surface distribution of accelerating column.

B. Initial parameters

There are a number of PIC codes developed for simulating space charge-dominated beam dynamics [20, 21]. Among them BEAMPATH can simulate unbunched continuous beam dynamics using the PIC method. Our simulation began with the point S (Fig. 1). A Gaussian distribution was assumed for a 20 keV axial symmetric deuteron beam. According to experimental data of the duoplasmatron ion source [22], initial parameters at S of deuteron beam were chosen as follows: beam envelope radius, $X = Y = 10$ mm; divergence angle, $X' = Y' = 50$ mrad; natural emittance, $\varepsilon = 150$ mm mrad; and normalized beam emittance, 0.7 mm mrad. The $E(z, r)$ field map of the accelerating column was calculated using the POISSON/SUPERFISH, and inputting into the BEAMPATH and IONB1.0, respectively. Beam intensity was set to 30 mA and 0 mA for considering and ignoring the space charge effect, respectively, when BEAMPATH was used. For IONB1.0, the space charge compensation had a significant impact on simulation results. In our previous study, fully unneutralized beam was assumed in the accelerating zones,

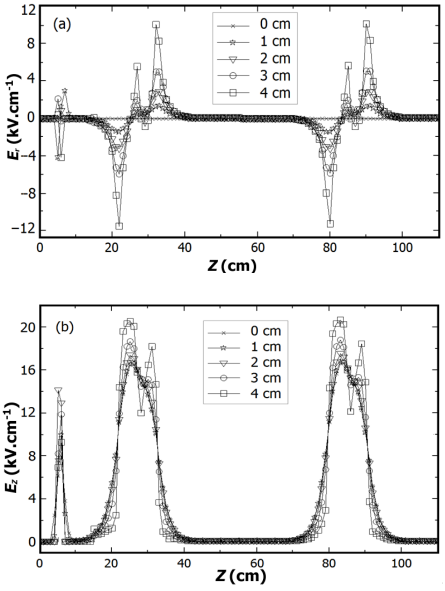

Fig. 4. Radial field maps of (a) $E_r(z,r)$ and (b) $E_z(z,r)$.

with the space charge compensation factor of 0.8 in the non-accelerating zones [17], but it should be 0.65 in the non-accelerating zones and 0 in the accelerating zones, comparing the simulation results of IONB1.0 with the BEAMPATH results.

C. Simulation results

The charged particle motion in electrostatic accelerating column depends on the external electrostatic field and the space charge self-field, and the space charge force causes beam divergence and emittance growth. The simulation results indicate that the deuteron beam of 30 mA can go through the accelerating column successfully.

The simulation results with space charge effect are shown in Fig. 5(a). The maximum of beam envelope radius at accelerating column exit is about 2.5 cm using IONB1.0, and the beam envelop radii of the vast majority of deuterons at accelerating column exit are 2–3 cm using BEAMPATH; while without space charge effect (Fig. 5(b)), the maximum of beam envelope radius at accelerating column exit is about 1.2 cm, and the beam envelop radii of the vast majority of deuterons at accelerating column exit are −1.2 cm. The beam divergence and the maximum of beam envelope radius are significantly less than those in Fig. 5(a).

Figure 6(a) illustrates the oscillation of the emittance along the accelerating column of both deuteron beam of 0 mA and 30 mA. Significant beam emittance growth can be seen in the BEAMPATH simulation. The beam emittance of 0 mA differs from that of 30 mA in the accelerating zones, and they vary differently in different accelerating zones. The beam emittance at the accelerating column exit is 0.3 cm mrad, being 4.3 times greater than the original emittances. As shown in Fig. 6(b), the space charge effect plays a significant role

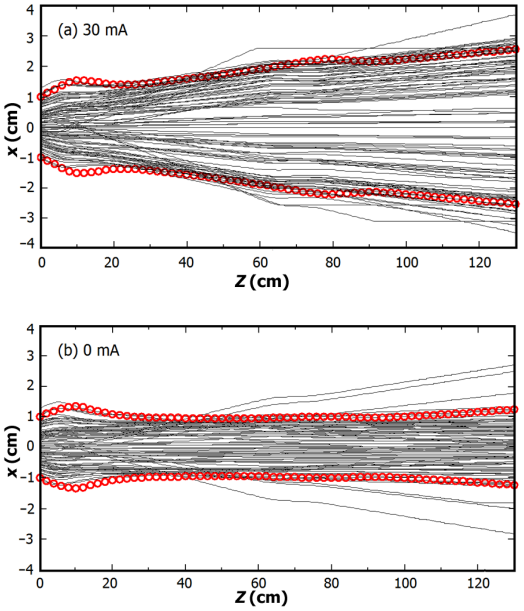

Fig. 5. (Color online) Envelopes along the accelerating column (a) with (30 mA) and (b) without (0 mA) space charge effect; the lines with red circle represent the simulation envelopes used IONB1.0, and the solid black lines represent the simulation envelopes used BEAMPATH.

in the beam emittance growth in the accelerating zones, the maximum of $\varepsilon_{30}/\varepsilon_0$, which is the beam emittance ratio of 30 mA to 0 mA, is 1.24 in the accelerating zones, but it is nearly 1 in the non-accelerating zones. This shows that the beam emittance increased rapidly before the beam incident to A1, inhibited in A1, and decreased in A2.

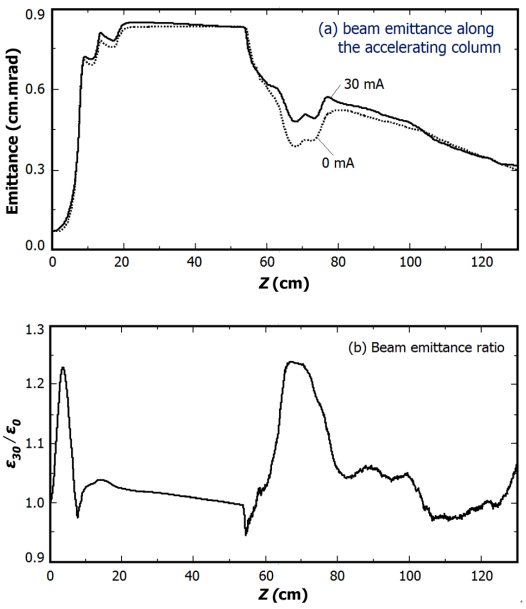

Fig. 6. Variation of beam emittance along accelerating column (a) and beam emittance ratio of 30 mA to 0 mA (b).

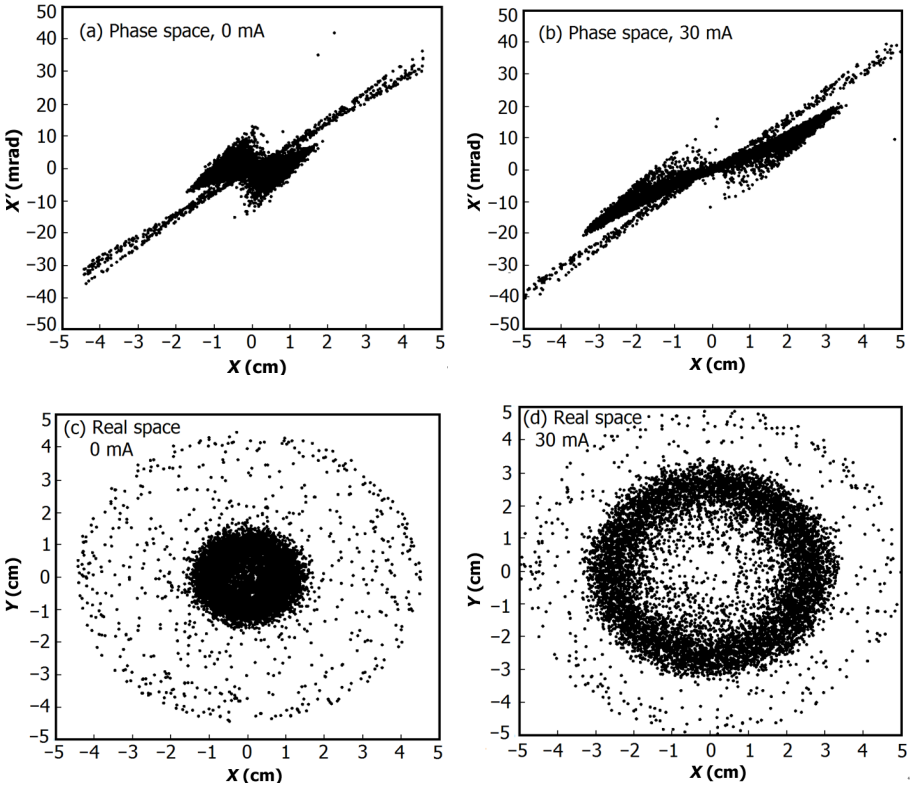

Fig. 7. Deuteron distributions in phase space at the accelerating column exit, (a) without (0 mA) and (b) with (30 mA) space charge effect; and in real space at the accelerating column exit, (c) without (0 mA) and (b) with (30 mA) space charge effect.

Figure 7 shows the final deuteron distributions in phase space or real space, without or with the space charge effect. With the space charge effect, the beam divergence increases (Figs. 7(a) and 7(b)) and the hollow beam is formed (Figs. 7(c) and 7(d)). An annular distribution is formed by a large number of deuterons, with the inner radii of about 2 cm and the outer radii of about 3 cm (Fig. 7(d)) at the accelerating column exit, indicating that the electrostatic accelerating column can transport space charge-dominated beam of 30 mA, as required by the design.

V. CONCLUSION

The transport of high-intense beam in the electrostatic accelerating column with two gaps was simulated by BEAMPATH and IONB1.0. The results show that the strong focus performance of the accelerating column and high gradient electric field can effectively cancel out ion beam divergence caused by the space charge effect, and the accelerating column can satisfy the requirement for intense D-T/D-D neutron generator.

[1] Carminati F, Klapisch R, Revol J P, *et al*. An energy amplifier for cleaner and inexhaustible nuclear energy production driven by a particle beam accelerator. CERN-AT-93-47-ET. http://cds.cern/ch/record/256520

[2] Li C K, Ma Y J, Tang X B, *et al*. Research of accelerator-based neutron source for boron neutron capture therapy. Nucl Tech, 2013, **36**: 1–6. (in Chinese) DOI: 10.11889/j.0253-3219.2013.hjs.36.090203

[3] Zhu F, Peng Z H, Hu Y M, *et al*. Physics design of heavy-ion irradiation beam line on HI-13 tandem accelerator. Nucl Tech, 2014, **37**: 22–26. (in Chinese) DOI: 10.11889/ j.0253-3219.2014.hjs.37.020204

[4] He X Z, Yang G J, Long J D, *et al*. Physics design of a compact medical cyclotron. Nucl Tech, 2014, **37**: 15–19. (in Chinese) DOI: 10.11889/j.0253-3219.2014.hjs.37.010201

[5] Wei Z Q, Sun K K, Sun Q Y, *et al*. Development in facility and technique of treating tumor with heavy ion beams. Nucl Tech, 2008, **31**: 53–57. (in Chinese)

[6] Yao Z E, Yue W M, Luo P, *et al*. Neutron yield, energy spectrum and angular distribution of accelerator based T(d,n)4He reaction neutron source for thick target. Atom Energy Sci Technol, 2008, **42**: 400–403. (in Chinese)

[7] Heikkinen D W and Logan C M. RTNS-II: Present status. IEEE Trans Nucl Sci, 1981, **28**: 1490–1493. DOI: 10.1109/TNS.1981.4331449

[8] Batygin Y K. Particle-in-cell code BEAMPATH for beam dynamics simulations in linear accelerators and beamlines. Nucl Instrum Meth A, 2005, **539**: 455–489. DOI: 10.1016/j.nima.2004.10.029

[9] Xiao C, Yuan Y J, He Y, *et al*. PIC mode simulation of solenoid collimation channel. Chin Phys C, 2010, **34**: 1136–1139. DOI: 10.1088/1674-1137/34/8/019
[10] Yang Y, Liu Z W, Zhang W H, *et al*. Simulation of a low energy beam transport line. Nucl Sci Tech, 2012, **23**: 83–89. DOI: 10.13538/j.1001-8042/nst.23.83-89
[11] Goncharov A. The electrostatic plasma lens. Rev Sci Instrum, 2013, **84**: 1–14. DOI: 10.1063/1.4789314
[12] Zhao G J, Ling B J and Xue K X. Optics of ions and electrons. Beijing (China): National Defense Industry Press, 1994, 98–106. (in Chinese)
[13] Reiser M. Theory and design of charged-particle beams. New York (USA): Wiley, 2004, 187–197.
[14] Batygin Y K. Conservation of space-charge-dominated beam emittance in a strong nonlinear focusing field. Phys Rev E, 1996, **53**: 5358–5364. DOI: 10.1103/PhysRevE.53.5358
[15] Kapchinsky I M and Vladimirsky V V. Proceedings of international conference on high energy accelerators and instrumentation, CERN, 1959, 274–288.
[16] Sacherer F J. RMS envelope equations with space charge. IEEE T Nucl Sci, 1971, **18**: 1105–1107. DOI: 10.1109/TNS.1971.4326293
[17] Lu X L, Yang Y, Yao Z E, *et al*. Design of 400 kV intense neutron generator. Atom Energy Sci Technol, 2012, **46**: 1473–1479. (in Chinese)
[18] Billen J H and Young L M. Poisson/superfish reference manual. Los Alamos National Laboratory, LA-UR-96-1834, 2003.
[19] Wartak A, Bereczky R J, Kowarik G, *et al*. Conceptual design and sample preparation of electrode covered single glass macro-capillaries for studying the effect of an external electric field on particle guiding. Nucl Instrum Meth B, 2015, **354**: 324–327. DOI: 10.1016/j.nimb.2014.12.055
[20] Chauvin N, Delferriere O, Duperrier R, *et al*. Transport of intense ion beams and space charge compensation issues in low energy beam lines. Rev Sci Instrum, 2012, **83**: 1–5. DOI: 10.1063/1.3678658
[21] Pande R, Singh P, Rao S V L S, *et al*. Optimization of solenoid based low energy beam transport line for high current H^+ beams. J Instrum, 2015, **10**: 1–11. DOI: 10.1088/1748-0221/10/02/P02001
[22] Sun B H and Chen Q. Characteristics of intense beam for a duoplasmatron source. Nucl Tech, 1991, **14**: 731–737. (in Chinese)
[23] Babu P S, Goswami A and Pandit V S. Optimization of beam line parameters for space charge dominated multi-species beam using random search method. Phys Lett A, 2012, **376**: 3192–3198. DOI: 10.1016/j.physleta.2012.08.031